Large-Area Gravure-Printed AgNWs Electrode on Water/Oxygen Barrier Substrate for Long-Term Stable Large-Area Flexible Organic Solar Cells[†]

Hao Wang,[a,b] Yaqin Pan,[a] Yunfei Han,*[a] Zhuo Chen,[a] Tianyu Liu,[a,b] Lianping Zhang,[a] Qun Luo,*[a] and Chang-Qi Ma*[a]

[a] *Printable Electronics Research Center & i-Lab, Suzhou Institute of Nano-Tech and Nano-Bionics, Chinese Academy of Sciences (CAS), Suzhou, Jiangsu 215123, China*
[b] *Nano Science and Technology Institute, University of Science and Technology of China, 166 Ren Ai Road, SEID SIP, Suzhou, Jiangsu 215123, China*

Keywords

Flexible organic solar cell | AgNWs electrode | Air storage stability | Barrier films substrate | Energy conversion | Flexible electronics | Interface

Comprehensive Summary
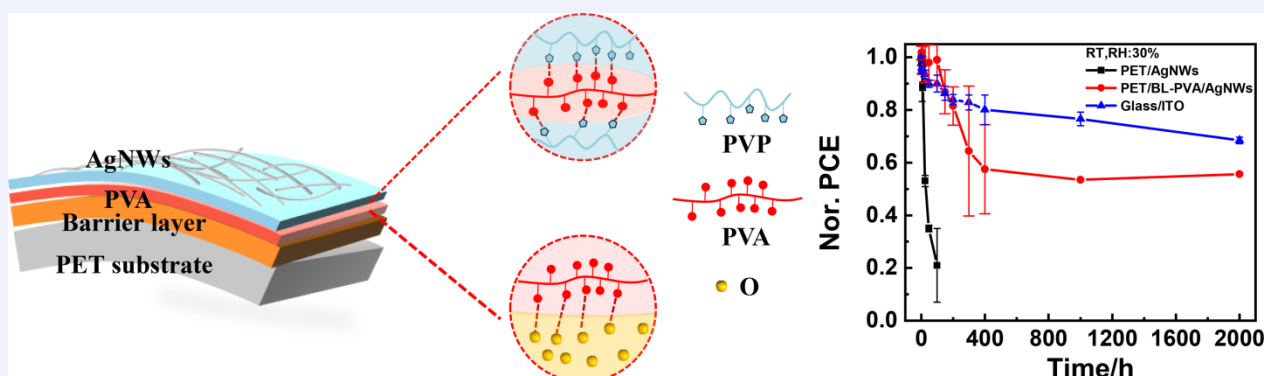
Large-area AgNWs electrodes (25 cm × 10 cm) were fabricated through roll-to-roll printing on the polyvinyl alcohol (PVA) modified water and oxygen barrier substrate. The modification of the barrier film with PVA improved the wettability of silver nanowires on the barrier films and led to the formation of homogenous large-area AgNWs networks. The mechanical flexibility, especially the adhesion force between the silver electrode and the barrier film substrate was dramatically improved through PVA modification. The efficiency of 13.51% for the flexible OSCs with an area of 0.64 cm^2 was achieved based on the PET/barrier film/PVA/AgNWs electrode. The long-term stability showed the flexible OSCs based on the PET/barrier film/PVA/AgNWs electrode have a significantly improved stability relative to the device on PET/AgNWs electrode, and comparable air stability as the rigid device with glass/ITO device. The unencapsulated devices maintained nearly 50% of the original efficiency after storage for 600 h in air. After a simple top encapsulation, the flexible devices remained at 60% of the initial efficiency after 2000 h in the air. Therefore, the flexible AgNWs electrode based on the barrier film would have the potential to improve the air storage stability of organic flexible solar cells.

*E-mail: yfhan2017@sinano.ac.cn; qluo2011@sinano.ac.cn; cqma2011@sinano.ac.cn
[†] Dedicated to the Special Issue of Organic Photovoltaic.

Background and Originality Content

Flexible organic solar cells (OSCs) have wide application prospects in building integrated photovoltaics[1-2] and wearable electronic devices[3-4] due to their advantages of lightweight,[5] high efficiency,[6-10] and flexibility.[6,8,11-17] In recent years, with the development of novel organic photoactive materials, the continuous breakthroughs in phase separation morphology optimization of the photoactive layer, and the in-depth exploration of the charge transport mechanism of the devices, the efficiency of flexible OSCs has been significantly improved.[6,18-20] The large-area (1 cm^2) organic solar cells based on flexible substrates have reached a power conversion efficiency (PCE) of 17.07%.[21] However, the storage stability of flexible OSCs has a big gap compared to devices on rigid substrates, and many factors lead to poor stability[22-27] of the flexible device compared to rigid OSCs which should be solved. Regarding the long-term stability of the flexible OSCs, rare efforts have been made.

For the flexible OSCs, we know the flexible transparent conductive electrode is a key that significantly influences both the performance and stability of devices. Among various flexible transparent electrodes, AgNWs have a comprehensive property of optical transparency, conduction, and mechanical durability.[28] With AgNWs as the flexible electrode, the device with high performance of over 17% has been reported.[21] In term of long-term stability, Kim *et al.*[29] compared the differences of efficiency and air stability between polyethersulfone (PES)/AgNWs electrodes and glass/ITO electrodes based on P3HT:PCBM active layer systems. Flexible OSCs with AgNWs and ITO electrodes stored in air under ambient conditions according to the ISOS-D-1 protocol (the devices stored in ambient conditions in the dark with periodic testing under AM1.5 G light) retained higher than 85% of the original efficiency after 30 d of storage. However, there was still a gap between silver electrode devices and ITO electrode devices in non-fullerene OSCs systems. Li *et al.*[8] found the flexible devices based on Em-Ag/AgNWs-SG and PET/ITO electrodes retained 60% and 61% of the initial efficiency, respectively, after exposure to air for 144 h. The oxygen and moisture resistance of Em-Ag/AgNWs-SG welding electrodes was comparable to that of ITO. However, the air storage stability of flexible OSCs was still lower than that of glass/ITO-based devices, which could retain 83% of the initial efficiency. This difference was mainly due to the poor water vapor transmission rate (WVTR) of PET relative to the ITO electrode.

In previous studies, the sandwich encapsulation strategy with simultaneous top and bottom encapsulation was usually used to improve the stability of flexible devices. However, the sandwich encapsulation structure would decrease the flexibility, and cause the complex imbalance of stresses during air storage after encapsulation. Recently, Brabec *et al.*[30] used the barrier film to encapsulate the top of the OSCs devices with a transparent conductive coating of ITO-Ag-ITO as the electrodes. Their results showed that the attenuation rate of different devices in the air was consistent, reflecting that the air stability of the device could be significantly improved after encapsulation. Therefore, it should be a possible strategy to improve the air stability of flexible devices through using the barrier films as the substrates.

In this work, AgNWs flexible transparent conductive electrode with high water and oxygen transmission rate was developed for long-term stable flexible OSCs. PET/barrier films were used as the flexible substrates. Due to the super-hydrophobicity of the barrier film surface, the surface modification with polyvinyl alcohol (PVA) layer was adopted to improve the wettability of the barrier film surface so that the high-quality and large-area AgNWs electrodes (25 cm × 10 cm) were fabricated by roll-to-roll gravure printing. The adhesion between the AgNWs electrodes and the barrier films was significantly improved after PVA modification, and the mechanical properties of the flexible electrode were enhanced. The device based on PET/barrier film/PVA/AgNWs electrodes had

an initial PCE of 13.51% with an area of 0.64 cm^2. The unencapsulated devices remained at about 50% of the initial PCE after being stored in air for 600 h, which was much higher than the devices based on PET/AgNWs electrodes and comparable to the rigid device based on the glass/ITO devices. Top-encapsulated devices based on PET/ barrier film/PVA/AgNWs electrodes were fabricated to further improve the stability of flexible OSCs.

Results and Discussion

To fabricate the flexible OSCs with good air stability, the PET films deposited with barrier layers were used as the transparent substrate. The water vapor transmission rate (WVTR) of the PET/barrier layer (PET/BL) substrate is 10^{-3} g·m^{-2}·d^{-1}, showing a potential use in flexible electronics. XPS of the barrier layer was measured to characterize the chemical structure of the barrier layer. The main elements in the barrier layer are C, O, Zn, and Sn as shown in Figure S1. To exclude the influence of the barrier layer on the transmission of the substrates, the transmittance spectra of the PET and PET/BL substrates were compared. As shown in Figure 1(a), the bare PET substrate showed high transmittance along the whole visible light region, with an average transmission around 90%. For the PET/barrier layer, there was a slight decrease in transmittance at the wavelength below 400 nm and above 800 nm due to the existence of a barrier layer. However, the PET/BL substrate also exhibited a transmission of over 80% at 550 nm.

Gravure printing is a high-speed printing process, which has shown great potential in the manufacture of large area electrodes and electron transport layers.[31] In this work, large-area AgNWs electrodes with the barrier layer as the substrates were fabricated through roll-to-roll gravure printing. Figure 1b shows the fabrication method of the AgNWs electrode by gravure printing. The flexible substrate is fixed on the rubber roller, and the silver nanowires ink is drip-dropped on the gravure roller. The silver ink on the cylinder is transferred to the rubber roller by high-speed rotation to obtain the AgNWs electrode. Both the PET/AgNWs electrodes and the PET/BL/AgNWs electrodes were fabricated through gravure printing without any pretreatment. As shown in Figures 1c—d, the PET/AgNWs electrodes were very uniform, while the PET/BL/AgNWs electrodes were uneven. There were many inhomogeneous and un-coverage areas of AgNWs on the PET/BL substrates, which were marked with the red circles in Figure 1d. For gravure printing, the film quality was highly influenced by surface properties of substrates. The PET/BL substrate is highly hydrophobic, which showed a larger water contact angle of 93.0° when water was dropped on the substrate. In contract, the PET substrate showed a smaller water contact angle of 59.0°. Since the AgNWs inks were dispersed in the composite solvent of water and ethanol, there would be poor wettability of this ink on the top the barrier films, which led to localized accumulation of AgNWs and inhomogeneous distribution. Further, the scanning electron microscope (SEM) images of the PET/AgNWs (Figure S2) and PET/BL/AgNWs films were measured and shown in Figures 1e—f. The results clearly showed that the AgNWs were seriously accumulated in some regions of the barrier layer, while they didn't cover in other regions of the barrier films.

In order to improve the wettability of the AgNWs inks on the top of the barrier layer and improve the film quality, the surface of barrier films was treated by ultraviolet-ozone (UVO) treatment. In addition, the interfacial modification strategy involving MD1200 and polyvinyl alcohol (PVA) materials, which were commonly used for treatment on PET or other flexible substrates, was also utilized through blade coating. The UVO irradiation and blade coating processes are shown in Figures 2a—b. To exclude the impact of these modification layers on the transmission of the substrate, the thickness of the MD1200 and PVA modification layers was optimized. As shown in Figure S3, the transmission of
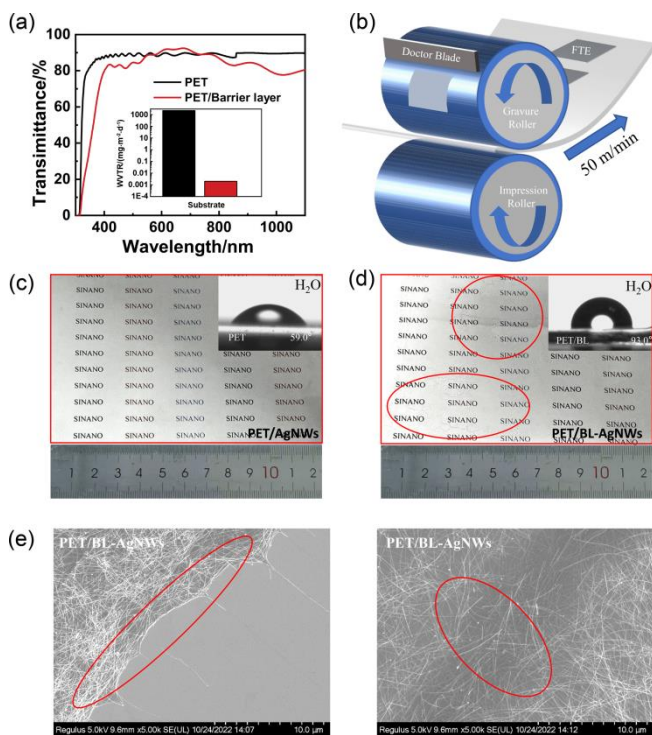
the MD1200-modified PET/barrier film of 50 nm thickness was slightly lower than that of the unmodified PET/barrier film in the 550—650 nm wavelength, but higher in the 650—1100 nm wavelength. The transmission of the MD1200-modified PET/barrier films of 70 and 90 nm thickness was slightly lower than that of the 50 nm film, while the overall transmission was still about 80%. The transmittance of PET/barrier films modified with different thicknesses of PVA was basically the same as that of unmodified PET/barrier films. These results showed the modification of MD1200 and PVA had a slight influence on the transmission of the

Figure 1 (a) The transmittance of PET and PET/BL substrate. (b) The schematic diagram of gravure printed AgNWs electrode. The large-area AgNWs electrode photographs and contact angle images based on (c) PET and (d) PET/BL substrate. (e—f) The SEM pictures of PET/BL/AgNWs electrode.

Figure 2 The schematic diagrams of (a) UVO treatment of the PET/BL substrates and (b) the blade coating that deposits the modification layer on the top of the barrier films. (c) The water droplet images on the surface of (d) UVO treated, (e) MD1200 modified, (f) PVA modified PET/BL substrates in different positions.
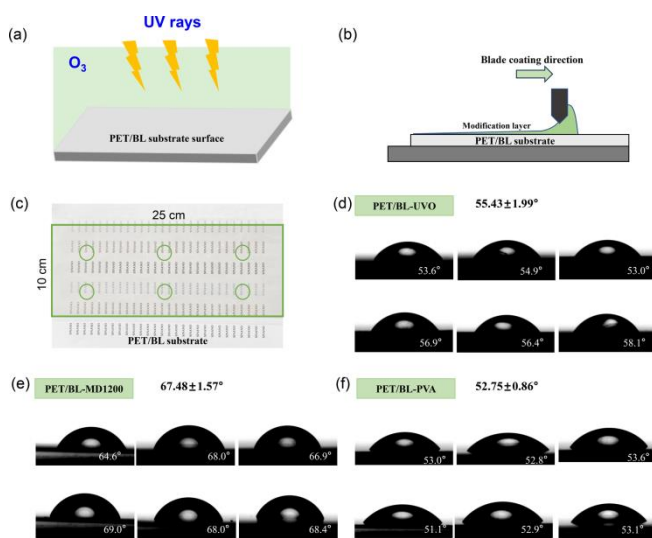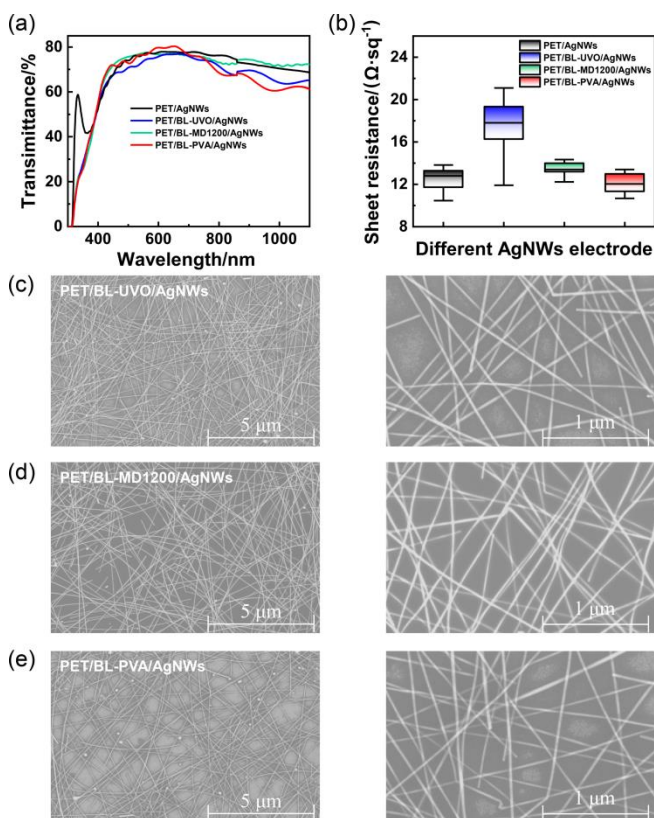
PET/barrier substrate.

To ensure the homogeneity of the treated barrier layer, the large-area PET/BL substrate with a size of 25 cm × 10 cm was fabricated (Figure 2c), and six different positions of the large-area PET/BL substrate were selected to evaluate the uniformity of surface energy through contact angle testing. Figures 2d—f show the water contact angle of PET/BL substrate with different treatment methods. The results showed that these three kinds of modifications have effectively improved the wettability of water on the barrier film surface. In detail, the contact angle of water on the surface of the modified barrier film was significantly reduced to 55°, 67°, and 53° after UVO treatment, MD1200 modification, and PVA modification, respectively. After PVA modification, the contact angle of water on the surface of the barrier film was the lowest, which symbolized the best wettability of silver ink on the PET/BL substrate surface. The deviation of the water contact angle of the UVO-treated films and MD1200 modified films is larger than that of the PVA modified films, and thus the surface energy of the UVO-treated films is not very uniform as the PVA modified electrodes. The error bars of the contact angles in different regions after PVA modification show the most uniform film quality. To further investigate the solvent resistance, the water contact angle of the PET/BL substrate washed by the water and methanol solvent was tested. As shown in Figure S4, the water contact angle remained almost unchanged after water and methanol washing, indicating that the MD1200 and PVA modified layer had good solvent resistance.

The AgNWs electrode was deposited on the barrier film through gravure printing by the method as our previous report.[21,31] The transmittance and sheet resistance of the PET/barrier/AgNWs electrodes based on different modification layers were characterized. As shown in Figure 3a, there are slight differences in the transmittance of the AgNWs electrode prepared on different modified substrates. The transmittance of the AgNWs electrode modified by UVO treatment and PVA modification is slightly lower beyond 800 nm. The sheet resistances of the AgNWs electrode based on different substrates were also tested. It can be seen that the sheet resistance of the PET/BL-UVO/AgNWs electrodes reaches up to 18 Ω/sq on average, and the uniformity is also the worst. The PET/BL-MD1200/AgNWs and PET/BL-PVA/AgNWs electrodes have similar sheet resistances of 12 Ω/sq, which are close to the sheet resistance of PET/AgNWs electrodes. The SEM images of the AgNWs electrodes on different substrates were measured. As shown in Figures 3c—e, the PET/BL-UVO/AgNWs electrodes showed morphology with slight agglomeration, which may be the reason for the larger sheet resistance. The PET/BL-MD1200/AgNWs and PET/BL-PVA/AgNWs electrodes are uniform and of good quality, indicating that the quality of the AgNWs electrode prepared on the surface of the barrier film is improved after the modification with MD1200 and PVA.

The flexibility and adhesion of the flexible transparent electrode are critical for the practical applications of flexible OSCs. The mechanical durability was evaluated *via* the ratio of R_{sh} to R_0 (where R_{sh} is the sheet resistance after bending, and R_0 is the initial sheet resistance) under 1000 continuous bending cycles with a radius of 5 mm. As shown in Figure 4a, the R_{sh} to R_0 ratio of the PET/BL-UVO/AgNWs electrodes increases to 30 after only 200 bending cycles. As expected, the R_{sh} to R_0 ratio of PET/BL-MD1200/AgNWs and PET/BL-PVA/AgNWs electrodes increases to 6 and 3, respectively, which is comparable to that of PET/AgNWs electrodes. The SEM images of AgNWs after 1000 bending cycles were measured. As shown in Figure S5, the barrier layer was cracked in the PET/BL-UVO/AgNWs films, indicating poor adhesion force between barrier films and PET substrates. The silver nanowires are deformed in the PET/BL-MD1200/AgNWs films. The PET/BL-PVA/AgNWs films and PET/AgNWs showed similar morphology as before bending. This result suggested the me-

chanical durability of the barrier layer could be improved with additional modification layers.


Figure 3 (a) The transmittance spectra and (b) sheet resistance of the PET/BL/modification layer/AgNWs electrode. The SEM images of (c) PET/BL-UVO/AgNWs, (d) PET/BL-MD1200/AgNWs, (e) PET/BL-PVA/AgNWs electrodes.

Furthermore, the peel test was carried out to evaluate the adhesion force between the barrier film and the AgNWs electrodes by using 3M tape. The sheet resistance of the AgNWs electrode was measured after 50 to 100 times peeling experiments, and the ratio of R_{sh} to R_0 was calculated, where R_{sh} and R_0 are the sheet resistance after peeling and the initial value. As shown in Figure 4b, the R_{sh} to R_0 ratio of PET/BL-MD1200/AgNWs dramatically increased to 4 after 20 cycles of the peeling test. The R_{sh} to R_0 ratio of PET/BL-UVO/AgNWs increased to 3 after 50 cycles peel test. However, the R_{sh} to R_0 ratio of PET/BL-PVA/AgNWs electrodes did not change much. The increase in sheet resistance indicated the fall of AgNWs, which might be due to the poor adhesion of AgNWs on the top of the barrier layer and MD1200 layer. This result suggested the adhesion strength between the barrier film and the AgNWs electrodes was significantly enhanced with the PVA modification layer.

The surface adhesion force of PET/BL-UVO, PET/BL-MD1200, and PET/BL-PVA films was tested using the 3M Tape Peel Test at 180° peeling angle. As shown in Figure 4c, the PET/BL-MD1200 and PET/BL-PVA films exhibited a higher adhesion strength with a peel strength of 70 N/m than PET/BL-UVO films with a peel strength of 60 N/m. This result indicates that the surface adhesion force of the barrier layer was enhanced after being modified by modification layers. Further, the interface adhesion force between AgNWs and different modification layers was also tested. As shown in Figure 4d, the peel strength of PET/BL-MD1200/ AgNWs and PET/BL-UVO films is 80 and 95 N/m, respectively. Compared with PET/BL-UVO/AgNWs and PET/BL-MD1200/AgNWs, the PET/BL-PVA/AgNWs films exhibited a higher adhesion strength (105 N/m). Herein, it is worth noting that the UVO

treatment and MD1200 modification can effectively improve the wettability of the AgNWs inks on the top of the barrier layer and improve the quality of the film, whereas the incompatibility of the barrier layer with the AgNWs caused weak interaction between the substrate and the AgNWs. These results demonstrate the PVA modification is effective to improve the adhesion force between the silver electrode and the barrier layer substrate. In the AgNWs electrodes, polyvinylpyrrolidone (PVP) is a kind of additive for regulating the dispersibility and film quality. Thus, hydrogen bond and van der Waals bond would be formed between the PVA and the AgNWs electrodes through PVP. These intermolecular forces would provide a strong adhesion interface and greatly improve the adhesion effect of AgNWs on the barrier layer. A possible mechanism of enhanced adhesion is drawn in Figure 4c.
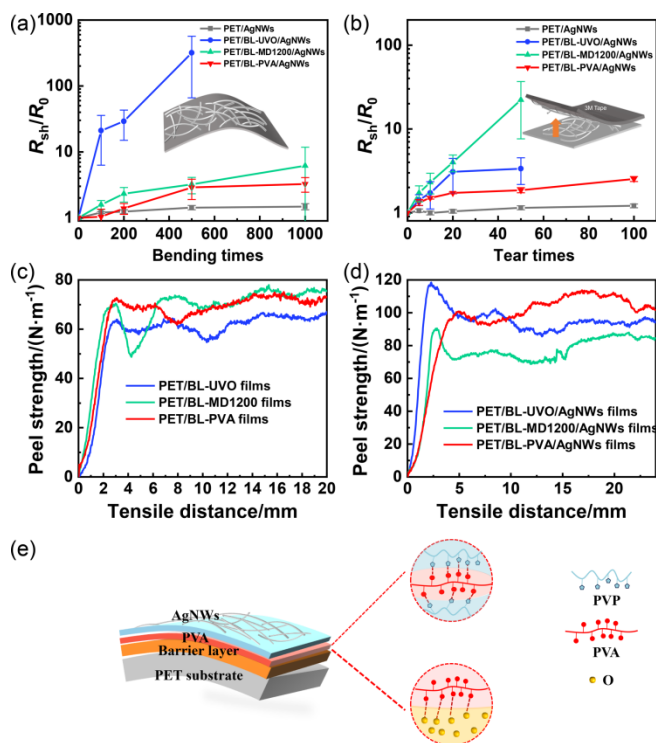
Figure 4 The sheet resistance variation of (a) after bending 1000 cycles, and (b) tearing via 3M tape based on PET/barrier layer/modification layer/AgNWs electrode. (c) The surface adhesion force of the barrier layer and (d) the interface adhesion force between AgNWs and different modification layers by the 3M tape peeling experiment. (e) Mechanism diagram of adhesion enhancement.

Flexible OSCs with an area of 0.64 cm^2 based on PET/BL/ AgNWs with different modified layers were fabricated. The inverted device structure and molecule structure of the organic donor and acceptor are provided in Figure 5a. The efficiency parameters of the devices based on different electrodes are exhibited in Table 1, and the *J-V* curves of the devices are shown in Figure 5b. The devices based on PET/BL-MD1200/AgNWs electrodes cannot work, which is due to the poor quality of the zinc oxide film on the MD1200. As shown in Figure S6, the surface of the PET/barrier/MD1200 electrode was cracked after the deposition of the ZnO layer. The device based on PET/BL-PVA/AgNWs electrode showed an open circuit voltage (V_{OC}) of 0.823 V, short circuit current density (J_{SC}) of 24.05 mA/cm^2, fill factor (FF) of 68.29%, and the champion power conversion efficiency (PCE) of 13.51%, which was close to 13.96% of the device efficiency based on the PET/AgNWs electrode. The J_{SC} of PET/BL-PVA devices is lower than the J_{SC} of PET/AgNWs devices due to the optical loss from the barrier layer. For the traditional encapsulation devices, additional adhesive layers and barrier films were required, which

would also reduce the transmission of incident light and reduce the performance of devices. For the PET/BL-PVA devices, no extra encapsulation was needed for the illumination side, such a small optical loss was acceptable for flexible OSCs. This observation indicated the AgNWs electrode printed on the PVA-modified barrier substrate is suitable for use in high-efficiency flexible OSCs.
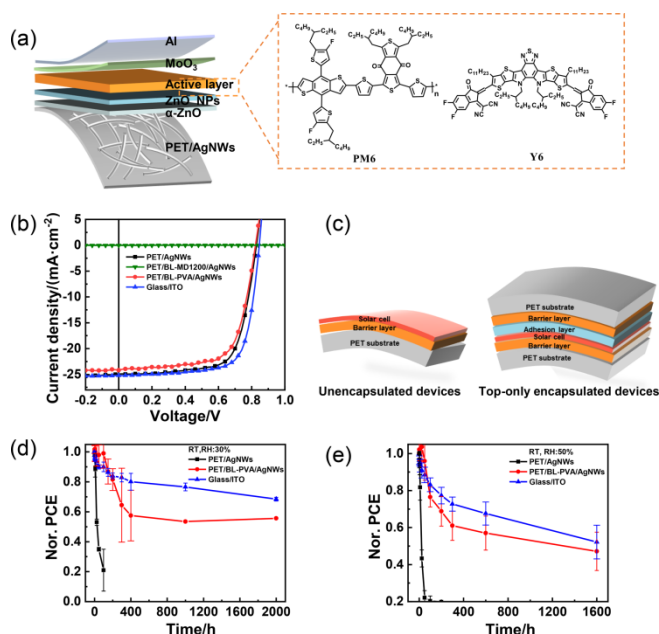
Figure 5 (a) The inverted flexible OSCs configuration and molecular structure of PM6 and Y6. (b) The J-V characteristics. (c) Schematic of un-encapsulated and top-only encapsulated devices. The air storage stability at a temperature of 25 °C and relative humidity of (d) 30% and (e) 50% for top-only encapsulated devices.

Table 1 The device performance parameters of flexible OSCs based on the PET/barrier layer/AgNWs electrodes with different modification layers

Electrode	V_{OC}/V	J_{SC}/(mA·cm^{-2})	FF/%	PCE/%
PET/BL-MD1200/AgNWs	—	—	—	—
PET/BL-PVA/AgNWs	0.823	24.05	68.29	13.51
	0.810±0.01	23.31±0.78	66.61±2.75	12.57±0.51
PET/AgNWs	0.828	24.94	70.26	14.51
	0.820±0.00	24.93±0.28	68.86±1.06	14.07±0.20
Glass/ITO	0.844	25.22	72.97	15.53
	0.837±0.00	24.80±0.43	71.53±1.46	14.85±0.45

After the fabrication of high-efficiency flexible OSCs on the top of the barrier layer, the operational stability and ambient shelf stability are studied. Firstly, the devices based on PET/AgNWs, PET/BL-PVA/AgNWs, and Glass/ITO electrodes show a similar operational stability trend under illumination in the N$_2$ glove box as shown in Figure S7. Then, the unencapsulated device was placed in a chamber with a constant temperature of 25 °C and relative humidity (RH) of 30%, and the efficiency change during this process was monitored. In order to further verify the air storage stability of the device, the side of the top electrode was encapsulated using the barrier layer with UV glue as the connection. In detail, UV glue was dropped on the top of the Al electrode, and the PET/barrier films were pasted on the Al electrode through the UV glue. After 5 min irradiation under UV light, the barrier layer was strongly connected to the flexible device. Figure 5c shows the structures of these two devices.

Figure S8 shows the efficiency degradation of the unencapsulated device stored in a constant temperature and humidity box at 25 °C and 30% RH. The device efficiency of the PET/AgNWs electrode decreases dramatically at the initial stage and rapidly

decreases to 20% after 200 h of storage. In contrast, the device efficiency of the PET/ BL-PVA /AgNWs electrode remains 70% of the initial value after 200 h of storage. At the initial stage of storage, devices based on PET/BL-PVA/AgNWs electrodes are more stable than ITO-based devices. The efficiency of both structures gradually degrades with a similar decay rate. Figures 5d—e show the efficiency attenuation of the top-encapsulated devices under the environment of a temperature of 25 °C and humidity of 30% RH and 50% RH. The other specific parameter changes of V_{OC}, J_{SC}, and FF are shown in Figure S9 and Figure S10. The top encapsulated devices with PET substrates still degraded fast both in the humidity of 30% RH or 50% RH, and the devices nearly cannot work after 100 h of storage. The efficiency of devices with PET/BL substrates degrades faster than the device with glass/ITO electrodes in the initial stage. As the storage time increases to 1600 h, the degradation rate of the glass/ITO and PET/BL/PVA/AgNWs devices became much slower. After 2000 h storage, the glass/ITO and PET/BL/PVA/AgNWs devices remained at nearly 70% and 60% of the initial efficiency when the environment humidity was 30%. In the case of HR 50%, around 50% of the initial efficiency remained for the glass/ITO and PET/BL/PVA/AgNWs devices.

Conclusions

In this work, large-area flexible transparent AgNWs electrodes with high air stability were developed through roll-to-roll printing with the PET/barrier layer as the substrate. Modification of the barrier film with a PVA layer was developed to improve the wettability of AgNWs and the barrier layer and enable the successful deposition of a uniform AgNWs network on the top of the hydrophobic barrier layer. The flexible electrode showed a reasonable transmission and sheet resistance of 80% and 12 Ω/sq, which was proven to be suitable for the use of high-performance flexible OSCs. Using this flexible electrode, high-efficiency and stable organic flexible OSCs were fabricated. It was found that the device prepared on the PET/barrier film/PVA/AgNWs electrode had comparable stability to the rigid device with glass/ITO as the electrode. The efficiency decreased to nearly 50% of the original efficiency after 600 h storage in the air, while the PET/AgNWs electrode-based device showed the fastest decay rate, and the device efficiency decayed to 40% of the initial efficiency after 50 h storage in air. After encapsulation of the top electrode, the device based on the barrier film/PVA/AgNWs electrode remained 60% of initial efficiency after 2000 h storage in air.

Experimental

Materials

Poly[[4,8-bis[5-(2-ethylhexyl)-4-fluoro-2-thienyl]benzo[1,2-*b*:4,5-*b*′]dithio-phene-2,6-diyl]-2,5-thiophenediyl[5,7-bis(2-ethylhexyl)-4,8-dioxo-4*H*,8*H*-benzo[1,2-c:4,5-c′]dithiophene-1,3-diyl]-2,5-thiophenediyl] (PM6) donor and Y6 acceptor were purchased from Solarmer Materials Inc., Beijing. Chlorobenzene (CB, 99.8%) and chloronaphthalene (CN) were purchased from J&K Scientific Ltd. Barrier film was purchased from YiTeOu New Materials Inc. PVA was purchased from Anhui Wanwei Group Co., Ltd. MD1200 was purchased from TOYOBO Co., Ltd.

Electrode fabrication

For the MD1200 modification layer, the MD1200 aqueous solutions were diluted by deionized water with different volume ratio (MD1200 : H$_2$O = 1 : 1, 4 : 1, 1 : 0). Then the MD1200 films were deposited on the surface of PET/barrier films through doctor blading (ZEHNTNER ZAA 2300) and annealed at 120 °C for 20 min. For the PVA-modified layer, the PVA material was dissolved in water at different concentrations (0.02, 0.05, 0.1, 0.2 mg/mL). Then PVA solutions were doctor-bladed onto the PET/barrier

layer films with the speed of 8 mm/s and annealed at 120 °C for 20 min. After that, the AgNWs network electrodes were deposited by gravure printing (D&R Lab Gravure Printer G-1100S, Suzhou D&R Instrum Co., Ltd.). The flexible substrate with a length of 33 cm and a width of 13 cm was attached to the imprinting roller. The cells of the patterned cylinder are then filled with the ink by the blade, and the ink is transferred onto the flexible substrate under pressure. Finally, the samples were baked at a temperature of 120 °C for 20 min. The effective area of electrodes is 25 cm x 10 cm.

OSCs fabrication

The OSCs of 0.64 cm^2 were fabricated with an inverted structure of PET/barrier layer/Modified layer/AgNWs/α-ZnO/ZnO NPs/Active layer/MoO$_3$/Al. To improve the wettability of AgNWs electrode surface, the AgNWs electrodes were treated by UV ozone for 5 min. The bilayer electron transport layers of α-ZnO and ZnO NPs were deposited according to the previous work.[32] The active layer inks were fabricated by dissolving the 8 mg/mL PM6 donor and 9.6 mg/mL Y6 acceptor together in chloroform with 0.5 vol% CN as an additive and stirred at 55 °C for 5 h in the glove box. The active layer inks were deposited onto the ZnO films at 3000 r/min for 30 s and active layer films were thermally annealed at 100 °C for 10 min. After annealing, the samples were transferred to the evaporation chamber. In the presence of a shadow mask, 10 nm MoO$_3$ and 200 nm Al were deposited on the samples under a vacuum of less than 1×10^{-4} Pa.

Characteristic

The WVTR of PET/BL films was measured using an electrolytic detection sensor (Coulomb-meter P205 sensor). XPS spectra of barrier layer films were measured using ESCALAB 250Xi spectrometer with a monochromatic Al Kα X-ray source with an overall energy space of ΔE = 0.1 eV. The transmittance spectra of the barrier film substrates and different electrodes were measured with the Lamada 750 UV-VIS-NIR spectrophotometer (PerkinElmer) under a standard measuring apparatus. The four-probe tester was used to test the sheet resistance of different electrodes. The bending and tearing test of electrodes was measured by recording the change in sheet resistance. The water contact angle of both the original barrier film and the modified surface was measured by a contact angle tester (JCY-1). The surface morphology of flexible electrodes was measured by using a scanning electron microscope (SEM, S4800). Current density-voltage (*J-V*) testing was performed in a nitrogen glove box using a solar simulator (100 mW/cm^2, XES-40S3) and a Keithley 2400 meter. The long-term storage stability of the unencapsulated and encapsulated devices was measured by testing the *J–V* curves after a period of storage in the air with controlled temperature and humidity.

Supporting Information

The supporting information for this article is available on the WWW under https://doi.org/10.1002/cjoc.202300479.

Acknowledgement

References

[1] Shen, Y.; Zhang, H.; Zhang, J.; Tian, C.; Shi, Y.; Qiu, D.; Zhang, Z.; Lu, K.; Wei, Z. In Situ Absorption Characterization Guided Slot-Die-Coated High-Performance Large-Area Flexible Organic Solar Cells and Modules. *Adv. Mater.* **2023**, *35*, 2209030.

[2] Min, J.; Bronnbauer, C.; Zhang, Z.; Cui, C.; Luponosov, Y. N.; Ata, I.; Schweizer, P.; Przybilla, T.; Guo, F.; Ameri, T.; Forberich, K.; Spiecker, E.; Bäuerle, P.; Ponomarenko, S. A.; Li, Y.; Brabec, C. J. Fully Solution-Processed Small Molecule Semitransparent Solar Cells: Optimization of Transparent Cathode Architecture and Four Absorbing Layers. *Adv. Funct. Mater.* **2016**, *26*, 4543–4550.

[3] Jin, W.; Ovhal, M.; Lee, H.; Tyagi, B.; Kang, J. W. Scalable, All-Printed Photocapacitor Fibers and Modules based on Metal-Embedded Flexible Transparent Conductive Electrodes for Self-Charging Wearable Applications. *Adv. Energy Mater.* **2021**, *11*, 2003509.

[4] Cui, N.; Song, Y.; Tan, C.; Zhang, K.; Yang, X.; Dong, S.; Xie, B.; Huang, F. Stretchable Transparent Electrodes for Conformable Wearable Organic Photovoltaic Devices. *npj Flex. Electron.* **2021**, *5*, 31.

[5] Wang, Y.; Chen, Q.; Zhang, G.; Xiao, C.; Wei, Y.; Li, W. Ultrathin Flexible Transparent Composite Electrode via Semi-embedding Silver Nanowires in a Colorless Polyimide for High-Performance Ultraflexible Organic Solar Cells. *ACS Appl. Mater. Interface* **2022**, *14*, 5699–5708.

[6] Zheng, X.; Zuo, L.; Zhao, F.; Li, Y.; Chen, T.; Shan, S.; Yan, K.; Pan, Y.; Xu, B.; Li, C. Z.; Shi, M.; Hou, J.; Chen, H. High-Efficiency ITO-free Organic Photovoltaics with Superior Flexibility and Upscalability. *Adv. Mater.* **2022**, *34*, 2200044.

[7] Liu, Y.; Zhang, J.; Gao, H.; Wang, Y.; Liu, Q.; Huang, S.; Guo, C. F.; Ren, Z. Capillary-Force-Induced Cold Welding in Silver-Nanowire-Based Flexible Transparent Electrodes. *Nano Lett.* **2017**, *17*, 1090–1096.

[8] Chen, X.; Xu, G.; Zeng, G.; Gu, H.; Chen, H.; Xu, H.; Yao, H.; Li, Y.; Hou, J.; Li, Y. Realizing Ultrahigh Mechanical Flexibility and >15% Efficiency of Flexible Organic Solar Cells via a "Welding" Flexible Transparent Electrode. *Adv. Mater.* **2020**, *32*, 1908478.

[9] Sun, Y.; Meng, L.; Wan, X.; Guo, Z.; Ke, X.; Sun, Z.; Zhao, K.; Zhang, H.; Li, C.; Chen, Y. Flexible High-Performance and Solution-Processed Organic Photovoltaics with Robust Mechanical Stability. *Adv. Funct. Mater.* **2021**, *31*, 2010000.

[10] Sun, W.; Chen, H.; Zhang, B.; Cheng, Q.; Yang, H.; Chen, Z.; Zeng, G.; Ding, J.; Chen, W.; Li, Y. Host-Guest Active Layer Enabling Annealing-Free, Nonhalogenated Green Solvent Processing for High-Performance Organic Solar Cells. *Chin. J. Chem.* **2022**, *40*, 2963–2972.

[11] Zha, W. S.; Gu, H. M.; Pan, W.; Sun, X.; Han, Y. F.; Li, Z. Y.; Weng, X. F.; Luo, Q.; Yang, S. F.; Ma, C.-Q. Controllable Synthesis and N-doping of HMoOx Nanoparticle Inks through Simple Photoreduction for Solution-Processed Organic Photovoltaics. *Chem. Eng. J.* **2021**, *425*, 130620.

[12] Zhang, X.; Wu, J.; Wang, J.; Yang, Q.; Zhang, B.; Xie, Z. Low-Temperature All-Solution-Processed Transparent Silver Nanowire-Polymer/AZO Nanoparticles Composite Electrodes for Efficient ITO-free Polymer Solar Cells. *ACS Appl. Mater. Interface* **2016**, *8*, 34630–34637.

[13] Zheng, Z.; Zhang, S. Q.; Wang, J. Q.; Zhang, J. Q.; Zhang, D. Y.; Zhang, Y.; Wei, Z. X.; Tang, Z. Y.; Hou, J. H.; Zhou, H. Q. Exquisite Modulation of ZnO Nanoparticle Electron Transporting Layer for High-Performance Fullerene-Free Organic Solar Cell with Inverted Structure. *J. Mater. Chem. A* **2019**, *7*, 3570–3576.

[14] Sun, Y.; Chang, M.; Meng, L.; Wan, X.; Gao, H.; Zhang, Y.; Zhao, K.; Sun, Z.; Li, C.; Liu, S.; Wang, H.; Liang, J.; Chen, Y. Flexible Organic Photovoltaics based on Water-Processed Silver Nanowire Electrodes. *Nat. Electron.* **2019**, *2*, 513–520.

[15] Dong, X. Y.; Shi, P.; Sun, L. L.; Li, J.; Qin, F.; Xiong, S. X.; Liu, T. F.; Jiang, X. S.; Zhou, Y. H. Flexible Nonfullerene Organic Solar Cells based on Embedded Silver Nanowires with an Efficiency up to 11.6%. *J. Mater. Chem. A* **2019**, *7*, 1989–1995.

[16] Xu, X.; Fukuda, K.; Karki, A.; Park, S.; Kimura, H.; Jinno, H.; Watanabe, N.; Yamamoto, S.; Shimomura, S.; Kitazawa, D.; Yokota, T.; Umezu, S.; Nguyen, T. Q.; Someya, T. Thermally Stable, Highly Efficient, Ultra-flexible Organic Photovoltaics. *Proc. Natl. Acad. Sci. U. S. A.* **2018**, *115*, 4589–4594.

[17] Bi, P. Q.; Zhang, S. Q.; Wang, J. W.; Ren, J. Z.; Hou, J. H. Progress in Organic Solar Cells: Materials, Physics and Device Engineering. *Chin. J. Chem.* **2021**, *39*, 2607–2625.

[18] Zhang, L.; Yang, F.; Deng, W.; Guo, X.; He, Y.; Zhou, J.; Li, H.; Zhang, Y.; Zhou, K.; Zhou, C.; Zou, Y.; Yang, J.; Hu, X.; Ma, W.; Yuan, Y. Organic–Inorganic Hybrid Cathode Interlayer for Efficient Flexible Inverted Organic Solar Modules. *Appl. Phys. Lett.* **2023**, *122*, 263903.

[19] Han, Y. F.; Chen, X. L.; Wei, J. F.; Ji, G. Q.; Wang, C.; Zhao, W. C.; Lai, J. Q.; Zha, W. S.; Li, Z. R.; Yan, L. P.; Gu, H. M.; Luo, Q.; Chen, Q.; Chen, L. W.; Hou, J. H.; Su, W. M.; Ma, C.-Q. Efficiency above 12% for 1 cm^2 Flexible Organic Solar Cells with Ag/Cu Grid Transparent Conducting Electrode. *Adv. Sci.* **2019**, *6*, 1901490.

[20] Han, Y.; Hu, Z.; Zha, W.; Chen, X.; Yin, L.; Guo, J.; Li, Z.; Luo, Q.; Su, W.; Ma, C. Q. 12.42% Monolithic 25.42 cm^2 Flexible Organic Solar Cells Enabled by an Amorphous ITO-Modified Metal Grid Electrode. *Adv. Mater.* **2022**, *34*, 2110276.

[21] Wang, Z. G.; Guo, J. B.; Pan, Y. Q.; Fang, J.; Gong, C.; Mo, L. X.; Luo, Q.; Lin, J.; Ma, C.-Q. Manipulating the Macroscopic and Microscopic Morphology of Large-Area Gravure-Printed ZnO Films for High-Performance Flexible Organic Solar Cells. *Energy Environ. Mater.* **2023**, e12592.

[22] Zhu, Y.; Kim, S.; Ma, X.; Byrley, P.; Yu, N.; Liu, Q.; Sun, X.; Xu, D.; Peng, S.; Hartel, M. C.; Zhang, S.; Jucaud, V.; Dokmeci, M. R.; Khademhosseini, A.; Yan, R. Ultrathin-Shell Epitaxial Ag@Au Core-Shell Nanowires for High-Performance and Chemically-Stable Electronic, Optical, and Mechanical Devices. *Nano Res.* **2021**, *14*, 4294–4303.

[23] Li, Y.; Mao, L.; Tang, F.; Chen, Q.; Wang, Y. X.; Ye, F. Y.; Chen, L.; Li, Y. W.; Wu, D.; Cui, Z.; Cai, J. H.; Chen, L. W. Ambient Stable Large-Area Flexible Organic Solar Cells Using Silver Grid Hybrid with Vapor Phase Polymerized poly(3,4-Ethylenedioxythiophene) Cathode. *Sol. Energy Mater. Sol. Cells* **2015**, *143*, 354–359.

[24] Lan, S.; Shin, H.; Kim, H. Electrically Stable Ag Nanowire Network Anodes Densely Passivated by a Conductive Amorphous InSnTiO Layer for Flexible Organic Photovoltaics. *Appl. Phys. Lett.* **2020**, *117*, 123303.

[25] Choo, D. C.; Kim, T. W. Degradation Mechanisms of Silver Nanowire Electrodes under Ultraviolet Irradiation and Heat Treatment. *Sci. Rep.* **2017**, *7*, 1696.

[26] Wang, P.; Jian, M.; Zhang, C.; Wu, M.; Ling, X.; Zhang, J.; Wei, B.; Yang, L. Highly Stable Graphene-Based Flexible Hybrid Transparent Conductive Electrodes for Organic Solar Cells. *Adv. Mater. Interfaces* **2021**, *9*, 2101442.

[27] Lee, S.; Lee, Y.; Lim, Y.; Han, J.; Jeon, I.; Bae, G.; Yoon, Y.; Song, W.; Myung, S.; Lim, J.; An, K.; Lee, S. High Energy Electron Beam Stimulated Nanowelding of Silver Nanowire Networks Encapsulated with Graphene for Flexible and Transparent Electrodes. *Sci. Rep.* **2019**, *9*, 9376.

[28] Yang, Y.; Xu, B. W.; Hou, J. H. Solution-Processed Silver Nanowire as Flexible Transparent Electrodes in Organic Solar Cells. *Chin. J. Chem.* **2021**, *39*, 2315–2329.

[29] Song, M.; Kim, J.; Yang, S.; Kang, J. Solution-Processed Silver Nanowires as a Transparent Conducting Electrode for Air-Stable Inverted Organic Solar Cells. *Thin Solid Films* **2014**, *573*, 14–17.

[30] Güler, E.; Distler, A.; Basu, R.; Brabec, C.; Egelhaaf, H. Fully Solution-Processed, Light-Weight, and Ultraflexible Organic Solar Cells. *Flex. Print. Electron.* **2022**, *7*, 025003.

[31] Wang, Z. G.; Han, Y. F.; Yan, L. P.; Gong, C.; Kang, J. C.; Zhang, H.; Sun, X.; Zhang, L. P.; Lin, J.; Luo, Q.; Ma, C. Q. High Power Conversion Efficiency of 13.61% for 1 cm^2 Flexible Polymer Solar Cells Based on Patternable and Mass-Producible Gravure-Printed Silver Nanowires Electrodes. *Adv. Funct. Mater.* **2020**, *31*, 2007276.

[32] Pan, W.; Han, Y. F.; Wang, Z. G.; Gong, C.; Guo, J. B.; Lin, J.; Luo, Q.; Yang, S. F.; Ma, C. Q. An Efficiency of 14.29% and 13.08% for 1 cm^2 and 4 cm^2 Flexible Organic Solar Cells Enabled by Sol–Gel ZnO and ZnO Nanoparticle Bilayer Electron Transporting Layers. *J. Mater. Chem. A* **2021**, *9*, 16889–16897.

The Authors

Left to Right: Hao Wang, Yaqin Pan, Yunfei Han, Zhuo Chen, Tianyu Liu, Lianping Zhang, Qun Luo, Chang-Qi Ma